Amaechi Paul, Obiakara (Orcid ID: 0000-0003-1093-1784)

Akala Andrew, Oke-Ovie (Orcid ID: 0000-0002-9754-9360)

Amory-Mazaudier Christine (Orcid ID: 0000-0002-5961-6331)

Geomagnetic activity control of irregularities occurrences over the crests of the African EIA

P. O. Amaechi[1, 2], E. O. Oyeyemi[2], A. O. Akala[2, 3, 4, 5], C. Amory-Mazaudier[6, 7]
[1]Department of Physical Sciences, Chrisland University, Owode, Abeokuta
[2]Department of Physics, University of Lagos, Yaba, Lagos, Nigeria
[3]Distance Learning Institute, University of Lagos, Akoka, Yaba, Lagos, Nigeria
[4]Maritime Institute, University of Lagos, Akoka, Yaba, Lagos, Nigeria
[5]The Abdus Salam International Centre for Theoretical Physics, Trieste, Italy
[6]Sorbonne Universités, LPP, Polytechnique, Paris, France
[7]T/ICT4D, ICTP, Trieste Italy

Corresponding author: Paul Amaechi (paoloobiaks@yahoo.fr)

Key points:

- Combined effect of PPEF and DDEF on ionospheric irregularities over the crests of the Africa EIA during intense storms.
- Hemispheric asymmetry in irregularities over the African EIA crests during the recovery phase of intense storms.
- Assessment of the predictive capability of the Prompt Penetration Equatorial Electric Field Model over Africa during intense storms.

This article has been accepted for publication and undergone full peer review but has not been through the copyediting, typesetting, pagination and proofreading process which may lead to differences between this version and the Version of Record. Please cite this article as doi: 10.1029/2020EA001183

Abstract

This paper investigated the behavior of ionospheric irregularities over the African Equatorial Ionization Anomaly (EIA) crests during intense geomagnetic storms which occurred from 2012 to 2015. Irregularities were monitored using the rate of change of TEC index (ROTI) along with variations of the horizontal component of the Earth's magnetic field (H) and ionospheric electric current disturbance (Diono). The predictive capability of the Prompt Penetration Equatorial Electric Field Model (PPEFM) was assessed by comparing prompt penetration electric field (PPEF) inferred from interplanetrary electric field (IEFy) and Diono with PPEF derived from the PPEFM, with emphasis on how well the model reproduced enhancement/reduction in the pre reversal enhancement (PRE). Eastward PPEF triggered short duration irregularities on 23 April 2012, 17 March 2013 and 20 February 2014 while westward electric field reduced them thereafter. The PPEFM rightly predicted enhancement (reduction) in PRE on 17 March 2013 (19 February 2014) when irregularities were triggered (inhibited). It however, showed no change in the PRE on 23 April 2012 and 20 February 2014. During the storms recoveries, irregularities were always inhibited/reduced over the trough by westward disturbance dynamo (DDEF) and the inhibition lasted longer during the super storm of March 2015. Also, there was a hemispheric asymmetry in irregularities over the African EIA crests. On 16-17 July 2012, 15 November 2012 and 19 March 2013, there were differences in irregularities behavior. On these days, the asymmetry of the post sunset crests was pronounced in both hemispheres.

1. Introduction

Ionospheric irregularities are small to large-scale structures that form in the plasma density (Pekins, 1975). Their interaction with Global Navigation Satellite System (GNSS) signals could result in rapid fluctuations in the amplitude and/or phase of the signals, giving rise to a phenomenon known as scintillation (Aarons, 1982; Datta-Barua et al., 2015). During intense scintillation conditions, GNSS signals might suffer degradation, reduction in their information content or failure in reception (Aarons et al., 1996; Kintner et al., 2007). The outcome could have disastrous effects on the life-critical GNSS applications especially, those utilized in navigation, positioning, search and rescue as well as military operations and surveying (Conker et al., 2003; Sunda et al., 2015). For this reason, adequate information about the actual state of the ionosphere is crucial for the smooth operation of the critical GNSS applications during all- weather conditions.

The low latitude ionosphere is mainly characterized by features such as the equatorial ionization anomaly (EIA) and ionospheric irregularities. The EIA results from the interaction of eastward electric field and the horizontal north-south geomagnetic field (Appleton, 1946; Namba & Maeda, 1939; Yue et al., 2015). Irregularities are generated by the generalized Rayleigh-Taylor instability (R-T instability) (Eccles, 2004; Farley et al., 1970; Yizengaw et al., 2013a) in the post sunset when plasma is further lifted up under the action of the pre reversal enhancement (PRE) in $\boldsymbol{E} \times \boldsymbol{B}$ drift velocities (Fejer et al., 1999). The plasma bubbles irregularities are depleted flux tubes which move upward, including the portion in the EIA crests (Groves et al., 1997). Parameters affecting the generation of irregularities are the: (i)

post sunset vertical drift, (ii) components of thermospheric winds, (iii) density gradient at the bottom side of the F-layer, and (iv) initial seed perturbations due to gravity wave from the lower atmosphere (Haerendel, 1973; Ott, 1978; Sultan, 1996; Tsunoda et al., 2013).

During solar disturbances such as geomagnetic storms, electrodynamics of the equatorial/low latitude ionosphere undergoes drastic variations. The equatorial region is mostly affected by mechanisms such as the prompt penetration electric field (PPEF) (Abdu et al., 2018; Abdu, 2012; Kikuchi et al., 2008; Scherliess & Fejer, 1997), and disturbance dynamo electric field (DDEF) related to winds driven by Joule heating and ion drag. The time of occurrence, the polarity and the combined effect of disturbed storm-time electric fields are therefore, crucial in controlling the variability of irregularities. PPEF has eastward (westward) polarity on the dayside (nightside) while DDEF is of opposite configuration (i.e. westward/eastward on the dayside/nightside) [Astafyeva et al., 2018; Blanc and Richmond, 1980; Yamazaki & Kosch, 2015]. Eastward (westward) electric field occurring in the post sunset can enhance (weaken) the regular eastward vertical plasma drift, thereby affecting the F layer rise (Fejer & Scherliess, 1995) and consequently the generation of irregularities (Aarons. 1991; Abdu, 2012; Kelley, 1989a; Shreedevi & Choudhary, 2017).

First evidence of geomagnetic disturbance on the horizontal component of the Earth's magnetic field (H) was presented by Chapman (1918). Later on, Nishida et al. (1966) and Nishida (1968) identified the disturbance polar no. 2 (DP2) current while Vasyliunas (1970) presented a theoretical model for magnetospheric convection. Manoj et al. (2008) postulated that the maximum propagation time for interplanetary electric field (IEF) to travel from the nose of the bow-shock to the equatorial ionosphere is about 17 minutes. Model results of Fejer and Scherliess (1997) revealed that PPEF vanished after 60 minutes due to the shielding effect of the ring current. However, cases of long lasting penetration electric field in the equatorial ionosphere during periods of enhanced magnetospheric activity and continuous southward Interplanetray Magnetic Field (IMF) have been reported (Huang et al., 2005; 2010). Huang (2019) recently showed that penetration electric fields dominated the equatorial plasma drifts for well over 14 hours, including 3 hours of the main phase and the first 11 hours into the recovery of the storm of December 2006. In line with the disturbance dynamo theory of Blanc and Richmond (1980), Le Huy and Amory-Mazaudier (2005, 2008) linked the magnetic signatures of the reversed solar quiet (Sq) current at low latitude to the ionospheric disturbance dynamo (Ddyn) which is the equivalent current system associated to DDEF.

Despite its wider spatial coverage over the low-latitude region, Africa has the fewer number of studies in terms of ionospheric response to storm-time electric fields. The lack of studies for Africa has been attributed to the long time absence of ionospheric observational tools over this sector (Paznukhov et al., 2012; Yizengaw et al., 2013b) which constitutes an impediment to global modeling. Over the last decade however, the availability of ground-based instruments thanks to projects such as the International Equatorial Electrojet Year (IEEY), the International Heliophysical Year (IHY) and the International Space Weather Initiative (ISWI) has helped in improving the knowledge the ionosphere over Africa.

For example, evidence of the inhibition of irregularities in Nairobi, Kenya and Kampala, Uganda has been presented during the storm of 6/8 April 2011 (Ngwira et al., 2013). Similarly, the suppressing effect of westward storm-time electric field on the PRE and the ensuing inhibition of irregularities over East Africa together with the reduction in the virtual height of the F2 layer (h'F2) (at Ascension Island) was presented by Azzouzi et al. (2015) for the October 2013 event. In addition, Ddyn and DP2 signals have been separated during several storms over Africa (Amaechi et al., 2018a; Azzouzi et al., 2015; Fathy et al., 2014; Nava et al., 2016). These works revealed characteristics of DP2 and Ddyn in terms of their source/origin, period, ionospheric responses and longitudinal behavior (Amory-Mazaudier et al., 2017) as well as amplitude, hemispherical behavior and asymmetry (Zaourar et al., 2017). Also, model studies using the Thermosphere-Ionosphere- Electrodynamics General Circulation Model (TIEGCM) (Carter et al., 2014) and the Prompt Penetration Electric Field Model (PPEFM) (Nayak et al., 2016) have been done to assess the ability of storm to enhance/ suppress irregularities and predict PPEF and its effect on irregularities, respectively. Such studies are more than ever needed over the African EIA during storms.

Despite all these works, a better understanding of the storm-time behaviour of ionospheric irregularities is still needed over the African EIA. Features such as their simultaneous response to PPEF and DDEF and the combination of both disturbed electric fields over the crests in both hemispheres are yet to be investigated during various storms. This poses not only a limitation to global modelling but also challenge to forecasting space weather which has long been the goal of the Space Physics and Aeronomy (SPA) community. This paper investigates variations of irregularities over the crests of the African EIA in both hemispheres during intense geomagnetic storms of the ascending phase of solar cycle 24. The study further performed for the first time over this region, comparison between PPEFs derived from ground based magnetometer data and inferred from the PPEFM (Manoj & Maus, 2012). To this end, section 2 describes the data sets and method of analysis while section 3 gives a highlight of the results obtained. The discussion and conclusion are presented in sections 4 and 5, respectively.

2. Data sets and Methods of analysis

2.1 Data sets

All storm events under investigation were associated with Coronal Mass Ejection (CME) [see the Solar and Heliospheric Observatory (SOHO)/Large Angle and Spectrometric Coronagraph (LASCO) CME Catalogue at https://cdaw.gsfc.nasa.gov/CME_list/ for a description of basic attributes of these events]. Their evolution in the interplanetary medium was monitored using the z component of interplanetary magnetic field (IMF Bz) and x component of the solar wind speed (Vx). Both data sets recorded onboard the Advanced Composition Explorer (ACE) satellite with time resolution of 64 seconds were time shifted by about 52 minutes to account for propagation delays to the Earth's magnetosphere (Chakrabarty et al., 2005). They were utilized to compute the y-component of interplanetary electric field (IEFy). Changes in the Earth's magnetosphere were examined using the symmetric H index (SYM-H) and horizontal component of the geomagnetic field (H). SYM-

H data were provided by the International Service of Geomagnetic Indices (ISGI). This data set with 1 minute resolution is more suitable for monitoring changes in the solar wind dynamic pressure (Wanliss & Showalter, 2006) and related current in the magnetosphere during storms. The ionospheric response vis-à-vis irregularities variation was analyzed using indices derived from GNSS observables.

H was computed using magnetometer data at the Addis Ababa station which is managed by the Institut de Physique du Globe de Paris (IPGP) and the data is distributed via the International Real-Time Magnetic Observatory Network (INTERMAGNET). GNSS observables for stations located in the African equatorial/low-latitude region around longitude 37^{o}E were obtained from University NAVSTAR Consortium (UNAVCO). These data with resolution of 30 seconds were used to estimate vertical total electron content (VTEC) and derive the rate of change of TEC index (ROTI). The coordinates of the magnetometer and GNSS stations are given in Table 1.

2.2 Methods of analysis

The y-component of the interplanetary electric field (IEFy) was estimated using the formula $IEF_y = -V_\times \times IMF\ Bz$ (Kelley, 1989b) where $V_\times$ and $IMF\ Bz$ are the x-component of the solar wind speed and z-component of interplanetary magnetic field, respectively. Also the horizontal component of the geomagnetic field (H) was computed using the north (X) and east (Y) components of the field (i.e $H = \sqrt{X^2 + Y^2}$). According to Cole (1966), the observed H is a combination of currents systems flowing in the magnetosphere-ionosphere (MI) system and is given by:

$$H = S_R + D \quad (1)$$

where S_R is the daily solar regular variation of the Earth's magnetic field associated to the regular ionospheric dynamo due to solar heating (Mayaud, 1965) and D is the integrated effects of disturbances coming from various current systems flowing in the Magnetosphere – Thermosphere system (Zaourar et al., 2017). S_R was estimated as the mean of H ($<H>$) during five most geomagnetically quiet days (n) in each month (i.e $<H> = \frac{1}{n}\sum_{i=1}^{n} H_i$). The quiet days were selected base on the criteria given by the GFZ German Research Centre for Geosciences.

Neglecting the effect of induced ground currents (Sabaka et al., 2004) as well as Chapman Ferraro currents (Chapman and Ferraro, 1931) and the tail currents in the presence of the generally strongest ring current, H can be written as:

$$H = < H > + DP + Ddyn + SYM\text{-}H \times cos\delta \quad (2)$$

where $SYM\text{-}H \times cos\delta$ is the symmetric component of the ring current and δ is the geomagnetic latitude of the station. DP is the disturbance polar currents (Kamide and

Fukushima, 1972; Nishida et al., 1966) and Ddyn is the ionospheric disturbed dynamo currents (Blanc and Richmond, 1980; Le Huy and Amory-Mazaudier, 2005).

The term DP + Ddyn is known as the ionospheric electric current disturbance (Diono) (Zaourar et al., 2017; Amory-Mazaudier et al., 2017). Diono combines the effects of: (i) the disturbance polar no.1 (DP1), (ii) disturbance polar no.2 (DP2), (iii) disturbance polar no.3 (DP3) and (iv) disturbance polar no.4 (DP4) as well as ionospheric disturbed dynamo currents (Ddyn). DP1 is one cell current system on the nightside associated with substorm (Rostoker, 1967, 1969) while DP2 is the one expanding from pole to equator due to convection electric field (Nishida, 1968). DP3 is a system of current flowing in the polar cap with direction opposite to that of DP2 (Kuznetsov & Troschichev, 1977; Troschichev & Janzhura, 2012). DP4 represents the current system of the disturbance related to the azimuthal component of IMF (Svalgaard, 1968). DP1, which is on the nightside is negligible along with DP3 and DP4 which are restricted to the polar cap (Stauning, 2012). Based on these, at middle and low latitudes we can write:

$$Diono = DP2 + Ddyn \quad (3)$$

DP2 is the equivalent current system due to PPEF (Nishida, 1968) and Ddyn is the equivalent current system associated to DDEF (Blanc & Richmond, 1980).

Using equations 2 and 3, Diono can then be derived as:

$$Diono = H - < H > - SYM\text{-}H \times cos\delta \quad (4)$$

Short-term oscillations of about 2 hours associated with southward turning of IMF Bz are the signature of DP2 [Nava et al., 2016] while diurnal oscillations are attributed to Ddyn (Le Huy and Amory-Mazaudier, 2005). In the equatorial region, Ddyn is absent at the beginning of the storm since it requires a few hours with respect to the start of PPEF and/or storm onset (Abdu, 2012; Huang 2013), typically 2-3 hours at nighttime, to get to the low latitudes. In this situation, DP2 becomes significant and can be approximated to Diono. Also, when a magnetic quiet day immediately follows a storm and there is no auroral activity and by implication weak convection electric field that is different from that during the storm, DP2 become zero and Ddyn can also be approximated to Diono (Amory-Mazaudier et al., 2017). Based on these, a running average filter that takes the mean value of 4 hours of Diono data with sliding of 1 hour was used for the separation of Ddyn from DP2 (Fathy et al., 2014; Azzouzi et al., 2015; Amaechi et al., 2018b). This method of separation and related assumptions remain valid only for short-duration PPEF (≤3 hours), but not during cases of long lasting PPEF. The filter nevertheless, is still useful in isolating Ddyn signal related to DDEF (which take typically 2-3 hours to reach the low-latitude after the beginning of the main phase). We therefore employed IEFy to further identify long-lasting PPEF. As such, when IEFy is eastward there is PPEF hence, DP2 occurs.

To gain more insight into variation of PPEF during the main phase of storms, the PPEFM was used to estimate PPEF in the African sector around longitude 37^{o}E. This model is mainly

a transfer function which models daily variations of equatorial ionospheric electric fields using interplanetary electric field (IEF) data mapped in the solar wind. Details about it can be found in Manoj and Maus (2012). The input parameters are time and location while the output parameters are estimated values of equatorial electric field (EEF) mainly the (i) background electric field (i.e quiet electric field obtained during geomagnetic quiet conditions) and (ii) total electric field (i.e the sum of quiet and prompt penetration electric fields).

GNSS observables in Receiver Independent Exchange (RINEX) format were subjected to quality check using the Translating Editing and Quality Checking (TEQC) software (Estey & Meertens, 1999). Relative Slant TEC (STEC) was thereafter estimated by leveling the carrier phase with the pseudorange measurements (Hansen et al., 2000). Prior to that, eventual cycle slips in the phase data were detected and corrected (Blewitt, 1990). Absolute STEC was derived from relative STEC by removing satellite and receiver biases (Sardon et al., 1994). This was finally converted to VTEC using a suitable mapping function with ionospheric pierce point (IPP) assumed at a height at 350 km (Mannucci et al., 1993). Details about TEC processing technique and software used can be found in Seemala (2010) and Seemala and Valladares (2011). The elevation cut off angle of 40^o was adopted in order to reduce multipath (Amaechi et al., 2018a) as well as to reduce errors related with varying IPP due to potential ionospheric gradients which are characteristic of the low latitude ionosphere (Rama Rao et al., 2006). The rate of change of TEC (ROT) was calculated, and converted to the unit of TECU/min according to equation 5.

$$ROT = \frac{STEC_k^i - STEC_{k-1}^i}{t_k - t_{k-1}} \times 60 \quad (5)$$

where *STEC* is in TECU, t_k is the time epoch, *i* is the visible satellite and $t_k - t_{k-1} = 30$ second.

The rate of change of TEC index (ROTI) was further computed as the standard deviation of ROT over 5 minutes (i.e $ROTI = \sqrt{< ROT^2 > - < ROT >^2}$) (Pi et al., 1997). ROTI is a good proxy for scintillation index (S_4) (Basu et al., 1999). In this work**,** ROTI values for all available satellites above the elevation of 40^o were averaged at a given epoch (5 minutes) (Jacobsen & Dähn, 2014; Amaechi et al., 2018a) and a threshold of 0.5 TECU/ min was set as the limit for the detection of irregularities (Ma & Maruyama, 2006).

The perturbation in TEC (ΔTEC) which is the difference between observed TEC and quiet TEC was computed for longitude 37^o with a latitudinal coverage of ±30^o and resolution of 1 hour x 1 degree (time/latitude). Quiet TEC was obtained by taking the average of VTEC during the 5 five most geomagnetically quiet days in the month. The day-to-day variability was taking care by computing the standard deviation of TEC during these quiet days. ΔTEC was hence, utilized to examine the contribution of the asymmetry of the EIA and its potential association with differences in irregularities variations especially on 16-17 July 2012, 15 November 2012 and 19 March 2013 when such differences were pronounced. The selection of storm events was done based on (i) their intensity (SYM-H < -100 nT) and (ii) season of occurrence and, (iii) simultaneous availability of GNSS data over stations located in both hemispheres.

3. Results

In this section each storm event has been analyzed using the SYM-H index, solar wind parameters (IMF Bz and IEFy), ground-based magnetometer data (H) and the derived current systems (Diono and Ddyn) as well as ROTI over stations in the crests and trough of the African EIA. All the storms were CME driven except case 1 which is a 'wake of CME' [www.spaceweather.com]. We included some days before and after the storms which acted as quiet time reference.

3.1 Storm case studies

Storm period of 23 – 24 April 2012

From Figure 1, the SSC (vertical dashed lines) occurred on 23 April (panel 1) while SYM-H reached a minimum value of -124.00 nT at 03:50 UT on 24 April. IMF Bz (second panel) went south with a minimum of -14.19 nT at 03:50 UT and turned north sharply. Thereafter, there was a long duration southward IMF Bz with a minimum of -15.30 nT at 17:40 UT. Prior to that there was another period of southward IMF Bz followed by a northward return at about 15:00 UT. Southward incursions were also observed on 24 and 25 April in the post sunset period. IEFy (third panel) was eastward with peak of 4.01 and 5.70 mV/m when IMF was southward on 23 April. The observed H (panel 4, red curve) had been superimposed on its quiet time reference level (blue curve) along with its day-by-day variation (light blue area). H clearly replicated the well-known regular pattern of the low latitude Sq for Addis Ababa. However, it increased and fluctuated at the time of SSC and was clearly below the limit of day-by-day variation in the post sunset period on 23 April as well as at about 04:30 UT on 24 April. Oscillations in H were also observed in the post sunset period on 24 and 25 April. Diono increased at the time of SSC (panel 5, mangenta curve) and fluctuated with minima on 23 – 25 April. Ddyn amplitude (panel 5, black curve) was undisturbed before the storm day. It decreased with minima on 23 – 25 April. (See Table 2 for the time of occurrence and magnitude of Diono and Ddyn minima). TEC irregularities were weaker over the trough and stronger over the crests with some hemispheric asymmetry especially before and after the main phase of the storm. On 23 April 2012, irregularities were inhibited over the trough (panel 7) and crests (panels 6 and 8) from 16:30 –18:00 UT (Figure 1, green rectangle), and subsequent triggering over the crests from exactly 18:00 UT. They remained inhibited on 24-25 April 2012.

Storm of 14 - 15 July 2012

Figure 2 is similar to Figure 1 but is for the storm of 15 July 2012. The SSC occurred at about 18:08 UT on 14 July 2012. SYM-H decreased gradually to -118.00 nT at 9:56 UT on 15 July and increased to -35.00 nT at 23:35 UT on 16 July. It decreased again to -75.00 nT at 07:10 UT on 17 July and finally recovered at a later time on 18 July. IMF Bz fluctuated south and north near the time of SSC with corresponding fluctuations in IEFy till pre-midnight on 14 July. A very long duration southward IMF Bz occurred from 06:00 UT on 15 July till 14:00 UT on 16 July with a minimum of -17.00 nT and related eastward IEFy of 11.23 mV/m at 07:50 UT. Another southward IMF Bz period occurred from 18:00 UT till the early hours of 17 July (IMF Bz = -8.95 nT at 03:46 UT and IEFy = 3.60 mV/m). Sudden increases in H and

Diono occurred at about 18:14 UT on 14 July. Thereafter, H decreased and was slightly below its limit of day-by-day variability at about 21:00 UT. This corresponded to a first Diono minimum. An obvious decrease of H with fluctuations and related minima in Diono occurred in the daytime and noon period on 15 -17 July. All stations experienced irregularities on 13 July. However, there was a weakening in their strength over the trough and reduction over the crests on 14 July 2012 and a complete inhibition over all stations on 15 July 2012. On 16 July, irregularities appeared over the southern crests (Figure 2, last panel, red box).

Storm of 13 - 14 November 2012

Figure 3 is also similar to Figure 1 but focuses on the storm of 13-14 November 2012. The SSC occurred at about 23:12 UT on 12 November while SYM-H reached a minimum of -114 nT on 14 November at about 08:00 UT. It then recovered gradually till 17 November. IMF Bz went south in the post sunset period of 12 November and reached a minimum of -17.71 nT at 23:30 UT on this day. It thereafter, fluctuated till the early morning of 13 November. H was clearly disturbed in the morning to noon period of 14 November. On this same day at about 03:02 UT, IMF Bz attained another minimum of -17.37 nT while both IEFy and Diono reached peaks of 7.23 mV/m and 50 nT, respectively. Ddyn also reached a peak but 2 hours earlier. Thereafter, Diono exhibited fluctuations with several minima from 06:00 ─ 10:00 UT while Ddyn reached its first minimum (still on 14 November). The magnitude of Ddyn reduced gradually from 14 – 16 November (Table 2). Weak irregularities were observed (10 and 12 November 2012) before the storm, with complete inhibition during the storm main phase (13 November) and first recovery day (14 November), followed by much stronger and asymmetric irregularities on 15 and 17 November.

Storm of 17 March 2013

Figure 4 is for the St. Patrick Day storm of 17 March 2013 characterized by a SSC at 06:00 UT and two SYM-H minima of -107 nT and -132 nT at about 11:56 UT and 20:30 UT, respectively on 17 March. SYM-H attempted a gradual recovered till about 19:53 UT on 20 March but decreased again to -61 nT at 03:43 UT on 21 March. IMF Bz went south, then north and south again with minima of -15.5 nT (at 05:30 UT) and -17.73 nT (at 07:20 UT) on 17 March. From 14:35 to 21:00 UT, it went on another southward journey with a minimum of -11.09 nT at 17:45 UT. During this period, IEFy was eastward with a peak of 11.90 mV/m. IMF Bz was southward for a short period in the pre-midnight of 20 March and early morning of 21 March. The respective minima were -7.18 mV/m and -7.22 mV/m. H was undisturbed on 16 March whereas on 17 March, it was clearly perturbed with fluctuations and several minima. On 18 March, it remained below the limit of day-by-day variation while on 19-21 March, it returned to its quiet time behavior. Similarly, Diono and Ddyn amplitudes were marked by minima on 17 to 18 March. Irregularities were triggered earlier (17:00 – 21:30 UT) over trough and crests (Figure 4, red rectangle) on 17 March 2013. They were reduced on 18 and 20 March while they reappeared on 21 March 2013 over all stations. On 19 March 2013, nevertheless, (Figure 4, green ellipse) only the southern crest experienced stronger irregularities.

Storm of 28 – 29 June 2013

Figure 5 has the same features as Figure 1 but deals with the storm of 29 June 2013. A sharp increase in SYM-H occurred on 27 June at the time of SSC (14:40 UT) with another increase at about 04:00 UT on 29 June. At 06:45 UT on June 28, a minimum of -104 nT was reached. This long lasting storm was characterized by a very long duration (21 hours) southward IMF Bz and eastward IEFy from 07:10 UT on 28 June to 10:40 UT on 29 June. Minimum IMF Bz of -12.33 nT with corresponding IEFy peak of 4.75 mV/m was registered at about 19:00 UT on 28 June. The H component was slightly below the limit of day-by-day variability at about 09:50 UT on 25 June. At the time of SSC it experienced a very weak impulse. From about 14:00 UT on 28 June to 03:38 UT on 30 June, it was clearly disturbed. Minima in Diono and Ddyn occurred on 26 June and 28 – 29 June. Weak and asymmetric TEC irregularities were observed over the trough and crests on practically all the days except on 29 June.

Storm of 19 – 20 February 2014

Figure 6 is for the storm of 19 February 2014. Salient features of this event are the three storm onsets which occurred on 19, 20 and 23 February (see broken lines) as well as SYM-H minima of -127 nT at 08:25 UT (19 February); and -100 nT and -93 nT at 05:53 and 11:53 UT (20 February). The first impulse was due to a CME while the second was triggered by the solar filament eruption of 18 February. IMF Bz turned southward with minima of -14.51 nT at 03:48 UT and -10.39 nT at 12:00 UT on 19 February. The second turning was however, followed by a sharp return to the northward configuration. Other southward conditions occurred on 20 February (minima of -10.68 nT, -7.72 nT, and -5.19 nT at 05:07 UT, 09:53 UT and 18:16 UT, respectively). The last southward IMF Bz condition took place from 14:00 – 17:00 UT with a minimum IMF Bz of -10.26 nT at 17:30 UT on 23 February and corresponding SYM-H of -50 nT at about 20:00 UT. H was below it limit of day-to-day variability from about 18:00 – 24:00 UT with an associated increase in Diono on 18 February. On 19-20 February however, H was clearly perturbed with oscillations and minima and corresponding conspicuous Diono and Ddyn minima in the noon period. The minima persisted from 21 to 23 February while H remained mildly disturbed. Strong (weak) but asymmetric TEC irregularities were observed over the crests (trough) on 17 – 18 February 2014. On 19, 21 and 22 February they were however, absent while they reappeared on 20 and 23 February 2014.

Storm of 17 March 2015

The St. Patrick's Day storm of 17 March 2015 has received considerable attention. As such, interplanetary and magnetic conditions during this event have been described in several literatures (e.g. Amaechi et al., 2018a,b; Borries et al., 2016; Nava et al., 2016; Nayak et al., 2016). The SSC started on 17 March at about 04:40 UT. SYM-H reached minima of -101 nT and -228 nT at 09:34 UT and 22:57 UT respectively. IMF Bz went south twice within 06:00 – 09:00 UT with minima of -21.06 nT and -20.83 nT at about 06:00 UT and 09:00 UT respectively, and corresponding peak eastward IEFy of 10.9 nT and 11.96 nT. It latter went on a long duration southward journey from noon to midnight with a minimum of -26.57 nT at

12:40 UT. H was disturbed on 17 March with several minima at 09:50 UT, 16:51 UT and 19:40 UT and on 18 - 19 March from 09:00 on March 18 to 15:00 UT on March 19. Diono exhibited oscillations with minima on 17 March as well as from 18 - 20 March while Ddyn also reached minima on these days. There were TEC irregularities on 16 March as well as on 20 -21 March 2015. On 17 -19 March 2015 however, the irregularities were inhibited at all stations. Overall, some hemispheric differences in TEC irregularities were observed over the crests. In effect irregularities appeared over the southern crests only on 16 July 2012 (Figure 2, last panel, red box) and 19 March 2013 (Figure 4, green ellipse) as well as on 15 November 2012.

3.2 Model representation of PPEF during the storms

Figure 8 presents variations of PPEF derived from the PPEFM during the main phase of the storms. The day after the main phase was included to account for long duration PPEF. PPEF + Quiet EEF (red line) has been superposed to Quiet EEF (dark line) obtained by taken the average of the 5 quietest days. The standard deviation of EEF during these quiet days was taken as the day-to-day variability. IEFy was eastward in the post sunset period of 23 April 2012 (Figure 1), 17 March 2013 (Figure 4) and 20 February 2014 (Figure 6) while Diono fluctuated and exhibited minima implying the presence of PPEF. PPEFM however, showed enhancement in the PRE on 17 March 2013 only (Figure 8d). Conversely, it successfully captured the reduction in the PRE when IEFy was westward in the post sunset on 19 February 2014 (Figure 8f). The model rightly predicted PPEFs on 24 April 2012 (07:30 – 08:00 UT), on 15 July 2012 (07:15 – 09:00 UT), 13 November 2012 (01:00-03:00 UT), 14 November 2012 (around 12:00 UT), 29 June 2013 (at about 14:00 and 20:00 UT) as well as on 17 March 2013 and 2015. During these events, IEFy was eastward while variations of Diono indicated the presence of PPEFs. On the other hand, oscillations in the quiet + PPEF curve on 23 April 2012 (at about 01:30 UT and 07:30 UT) and 28 June 2013 (01:00-03:00 UT) could not be attributed to PPEF given that IEFy was westward immediately before the initial phase. On the contrary, the fluctuations on 19 and 20 February from 07:00 – 14:00 UT (Figure 8f) were indication of PPEFs. Interestingly, the PPEFM showed penetration of electric field in the early hours of 18 March 2015 during the recovery phase. This period corresponded to a return of IMF Bz to northward while H was still disturbed and AE index (not shown) indicated auroral electrojet activity till about 01:30 UT. During the very long duration of southward IMF Bz and related eastward IEFy on 15-16 July 2012 and 28-29 June 2013, the model did not show any PPEF.

3.3. Variations of TEC

Figure 9 shows TEC perturbation along mean longitude 37^{o} on days when differences in irregularities behavior were observed over both crests. From the first panel, on 16 July 2012 there was a clear asymmetry in TEC with larger enhancements in the northern crest (southern crest) from 04:00 – 09:00 UT (09:00 -13:00 UT). In the post sunset, the enhancement was confined within the magnetic equator. On 15 November 2012, the perturbation was localized within the magnetic equator during noon *albeit* stronger in the northern hemisphere. The post sunset crests were enhanced and asymmetric. 19 March 2013 was relatively quiet although

noon enhancement could be observed in both hemispheres around the crests. However, there was only one crest in the post sunset period especially at about 17:00 UT (20:00 LT). The second panel of Figure 9 shows that ionization varied differently in the noon and post noon periods before and after the storm. It was more enhanced with well developed post sunset crest after the storm.

4. Discussion

It is well known storm time PPEF and DDEF can affect the regular electric field (ie, $\boldsymbol{E} \times \boldsymbol{B}$ drift) hence, the formation of ionospheric irregularities (Abdu et al., 2009, 2018). When IMF Bz turns south and convection electric field (IEFy) increases, PPEF whose signature is the DP2 signal can penetrate into the low-latitude ionosphere (Kikuchi & Akari, 1979). The disturbed electric field can be captured in the form of a perturbation in the H component and short-term oscillations of Diono (Nava et al., 2016) especially during the beginning of a storm (Amory-Mazaudier et al., 2017). However, the time of occurrence of PPEF is crucial in influencing the pattern of irregularities. For example, the presence of westward PPEF/ DDEF at about 18:00 UT (LT=UT+3 hours) on 17 March 2015 acted to suppress the PRE thereby inhibiting irregularities. Zakharenkova et al. (2019) observed intense post sunset equatorial plasma bubble (EPB) irregularities using measurement from SWARM satellite and ground-based GNSS along with stronger depletion in the Communications/Navigation Outage Forecasting System (C/NOFS) ion density over East Africa on 16 March 2015 and complete inhibition on 17 March during the main phase while DDEFs were active. In addition, westward electric field which had developed around 20:00 UT on 14 July 2012 acted to reduce the evolution of irregularities activity. Chakraborty et al. (2015) had previously observed that eastward IEFy was opposite to zonal electric field thus, failed to enhance the upward $\boldsymbol{E}\times\boldsymbol{B}$ plasma drift in the local night-time hour of the Indian sector on 14 July 2012. Also, some westward DDEF in the afternoon sector can affect the PRE hence the development of irregularities as was the case on 19 February 2014.

On the other hand, during the southward turning of IMF Bz that occurred at about 17:40 UT on 23 April 2012; the southward IMF Bz of 17 March 2013 at 17:35 UT as well as the not so large IMF Bz change at 18:16 UT on 20 February 2014, eastward PPEF enhanced the upward $E \times B$ drift thus, triggered short duration irregularities over the trough and crests on 23 April (Figure 1), on 17 March (Figure 4, red box) and in the pre-midnight period of 20 February 2014 (Figure 6). The result of 23 April 2012 is particularly interesting giving that irregularities were earlier inhibited by westward electric field (Figure 1, Green box). In line with our observations on 17 March, Kalita et al. (2016) found that short duration irregularities were triggered when IMF Bz turned south in the sunset period over 100^{o} E longitude. Also, Kassa and Damtie (2017) reported that irregularities were triggered in Bahir Dah (11^{o}N, 38^{o}E), Ethiopia by an enhanced drift which had favored the post sunset lifting of the F-layer (Joshi et al., 2015) to altitude where irregularities were generated by the R-T instability mechanism (Kelley, 1989b). Similar triggering of irregularities by eastward PPEF with corresponding deep density depletions and EPBs were captured using the Defense Meteorological Satellite Program (DMSP) and ground-based GNSS, respectively during the

main phase of the storm of 13 September 2004 in Africa (Ngwira et al., 2013). In line with these observations, Zakharenkova & Astafyeva (2015) reported that eastward PPPEF significantly enhanced CHAMP ROTI and increased the fluctuations level of ROT data from ground-based GNSS in Africa during the main phase of the storm of 30 August 2004.

Conversely, DDEF are more active during the recovery phase of a geomagnetic storm. The decay in H several hours after the beginning of the disturbance is the signature of Ddyn current system (Azzouzi et al., 2015) related to westward DDEF (Le Huy & Amory-Mazaudier, 2008). DDEF are driven by increased heating of the thermosphere at high latitude ensuing from the energy input during storms (Danilov & Lastovicka, 2001) and the resultant change in global circulation. Their presence in the post sunset period can inhibit the development of irregularities (Abdu et al., 1995). The minima in Ddyn in the post sunset is evidence of the presence of DDEF which might have inhibited irregularities over the crests and trough on 24-25 April 2012, 15-16 July 2012, 18 March 2013, 19 February and 21-22 February as well as 17 – 19 March 2015. Kassa and Damtie (2017) had similarly reported a sharp drop in irregularities level on 19 February 2014 and a prolonged suppression thereafter, over Bahir Dah while Zakharenkova et al. (2019) observed a complete inhibition of EPBs using SWARM and C/NOFS observations in conjunction with GNSS ROTI maps on 18 March 2015. It is important to note that the duration of irregularities inhibition lasted longer during the super storm of March 2015 (3 days) than the other storms (1-2 days). Although Ddyn lasted 6 days, its amplitude was well reduced from 20 -22 March (Nava et al., 2016). The magnetometer at Addis Ababa also showed a reduction in Ddyn amplitude on 20 March while there was no data 21 March. It is known that the necessary condition for the generation of post sunset irregularities is the rise of the F layer to higher height under the influence of PRE. It is thus very likely that the weak Ddyn on 19 -21 March 2015 were not efficient enough to prevent the rise of the F layer, which was controlled by higher drift velocity typical of months of high solar activity (Fejer et al., 1999).

Additionally, overshielding penetration electric field of westward polarity can occur when the southward IMF Bz is followed by a rapid turning to northward and there is rapid decrease in convection during the main phase (Kikuchi et al., 2000). Stressing further, Kikuchi et al. (2003) postulated that when R2-FACs build up following the rapid decrease in R1-FACs, due to the northward turning of the IMF and concomitant decreased in convection, electric field in the equatorial region reverse from eastward to westward under the so-called dominant shielding electric field (Kelley et al., 1979). From 15:00 – 18:00 UT on 23 April 2012, there were sharp fluctuations in IMF Bz with corresponding peak in westward IEFy. The westward overshielding electric field could have acted to suppress the PRE hence, inhibit irregularities from 17:00 – 18:00 UT. Another contributing factor could have been the existence of westward DDEF described in the previous paragraph. In fact, Chakraborty et al. (2015) reported enhancement of the AE index on 23 April 2012 at about 06:00 UT and 15:00 UT. These implied the presence of heating source at high latitude which may have led to the development of DDEF on this day. Recently, Huang (2018) confirmed that it takes about 4.7 hours after the onset of a storm for the effect of disturbance dynamo to reach the equatorial region. It is thus, inferred that westward electric field (overshielding electric field and DDEF)

were responsible for the inhibition of irregularities from 17:00 – 18:00 UT on 23 April (Figure 1, green box).

The occurrences of irregularities near the trough cannot be explained by electric fields only. The PRE occurs in the post sunset when solar photoionisation decreases rapidly, consequently there are large density gradients thus irregularities develop thanks to the R-T instability. Background density is thus, a crucial factor to reckon with in the formation of irregularities. The storm of November 2012 occurred during winter when irregularities are weak and their occurrence quite random (Akala et al., 2014). To examine the observed difference in irregularities before (10 and 12 November) and after the storm (15 and 17 November), we examined the TEC profile in the post sunset of 10 and 15 November (Figure 9, second panel). It was found that the crests were not well formed before the storm while they were well developed after it. Also, the dynamism of ionization on 10 November was not too different from that during quiet days. Therefore the difference in irregularities could be attributed to background ionization in addition to recombination processes. Oppositely, the inhibition of irregularities during the storm main phase (13 November) and first recovery day (14 November) was related to the presence of westward DDEF. Olwendo et al. (2015) identified westward electric fields using magnetic field variations (dH) during this storm.

The storm of June 2013 was particularly interesting with its long and smooth main phase, as well as slow changing dH/dt and asymmetric irregularities practically during all the days (Figure 5). This storm occurred in June solstice during which nighttime to post midnight irregularities are frequent (Akala et al., 2014; Yizengaw et al., 2013). In line with this, irregularities were observed from night to post midnight before the storm. On 28 June during the main phase, they were triggered in the post sunset by the long duration PPEF. On 29 June, westward DDEF prevented them from occurring. On 30 June however, the resurgence of post sunset irregularities might have been associated with the northward incursion of IEFy around 18:00 UT.

Fluctuations in Diono and Ddyn around 11 UT on 17 February when SYM-H, IMF Bz and IEFy were completely quiet were related to the reduction in H slightly below the day-to-day variability. This interesting phenomenon could have been caused by: (i) solar flare and /or (ii) westward electric field. In effect, four C class solar flares which were well above the background flux F B7.8 were emitted within 02:51 – 09:53 UT on 17 February. (https://www.spaceweatherlive.com/en/archive/2014/02/17/xray). Zhang et al. (2017) had shown that during flare events, enhancement in the cowling conductivity may modulate the ionospheric dynamo and decrease the EEF. On the other hand, there was increase in auroral activity and polar cap potential from 14:40 to 22:30 UT on 16 February (not shown in this paper). AE and AO indices reached 871 and -686 nT, respectively. The westward electric field generated by such disturbance might have lasted long enough to affect electric field on 17 February. Irregularities on 20 February were due to eastward electric field associated with the short lived southward IMF Bz incursion at 18 UT. On the other hand, their presence on 23 February (when we expected them to be inhibited because of the negative H, Diono and Ddyn) was related the northward incursion of IMF Bz when a IEFy penetrated to the

magnetic equator.

Ionospheric irregularities over Africa are less frequent in solstices because of the weaker drifts (Wiens et al., 2006; Yizengaw et al., 2014) associated with this season. They occur predominantly during equinox season (Oladipo et al., 2013; Paznukhove et al., 2012; Wiens et al., 2006) when there is a good alignment between the solar terminator and the geomagnetic meridian (Tsunoda, 1985). This scenario gives rise to increase in conductivity gradient hence, eastward electric field and the consequent optimum vertical drift needed to lift the F layer to altitude favorable for the development of irregularities (Eccles et al., 2015). Other studies have shown increase occurrence rate in March equinox than September equinox (e.g. Mungufeni et al., 2016; Oladipo et al., 2013; Olwendo et al., 2013) with some occurrences in summer (Akala et al., 2014). This seasonal behavior was well captured during our events, with stronger (weaker) irregularities during the April 2012 (July 2012/November 2012), and March 2013 (June 2013) events. During storm nonetheless, this expected seasonal pattern can be altered significantly under the dictate of electric field and the intensity of the ring current as shown earlier.

As for solar activity, it was observed that strongest irregularities (ROTI >3 TECU/min) occurred in February 2014 which also registered the highest solar flux (170.3 sfu), and weakest irregularities (ROTI < 0.5 TECU/min) in June 2013 with corresponding lowest solar flux (110.74 sfu). This was a fairly reflection of the solar activity control of irregularities whereby higher solar flux was associated with stronger irregularities (Aarons, 1991) in line with the increase in post sunset drifts with solar flux (Fejer et al., 2008). Previous studied have examined the solar activity control of quiet time irregularities over Africa (Akala et al., 2014; Mungufeni et al., 2016). During storm nevertheless, it was found that irregularities were generally inhibited during various solar cycle phases in line with past observations (Dugassa et al., 2020; Ngwira et al., 2013; Seba & Nigussie, 2016).

Previous work by Amaechi et al., (2018ab) had presented the effect of storms on irregularities near the magnetic equator. The present study emphasized on the simultaneous behavior of irregularities over the crests in both hemispheres and investigated plausible mechanism responsible for their behavior. Irregularities occurrence over the crests is quite complex and least studied over the African EIA. Ordinarily, EPBs generated at the magnetic equator extend along the magnetic field lines and the crests. Generally, irregularities were strong over the crests and weak over the trough during most of our events mainly because of the larger background ionization at the crests. Additionally, most TEC irregularities occur at roughly the same time over the crests and trough, indicating that they were from the same origin. However, there were differences in the irregularity behavior over the crests especially on 17 July 2012 and on 19 March 2013 which will be examined in the next section along with the TEC perturbation profile.

From Figure 2, it is evident that PPEF and DDEF acted on 16 July 2012. The eastward PPEF had modulated the enhancement in TEC from 06:00 – 12:00 UT (Figure 9, first panel). On the other hand, westward DDEF acted to reduce irregularities over all stations till 22:00 UT. TEC irregularities nonetheless, reappeared at the southern crest and trough but not at the

northern crest 22:00 – 24:00 UT on this day. From Figure 9 (first panel) maximum ionization was confined within the magnetic equator in the post sunset. On 15 November 2012, the presence of DDEF (with reduced amplitude) and the observed weak background ionization at the magnetic equator accounted for the presence of weak irregularities at the trough. ΔVTEC profile in the post sunset period showed enhancement in ionization an obvious hemispheric asymmetry in TEC (Figure 9, middle panel) which could have been responsible for the difference in TEC irregularities over both crests. On 19 March 2013 however, magnetic conditions were relatively quiet yet there was only one post sunset crest in the southern hemisphere (Figure 9, panel 3). This observed hemispheric asymmetry is indication of the presence of transequatorial neutral wind and other processes, such as composition change during the recovery phase. Maruyama & Matuura (1984) showed that various forms of plasma transport by wind from one hemisphere to another can affect conductivity thus, the instability growth rate. Nicolls et al. (2006) had noted that even in the presence of westward electric field, a contribution from meridional equatorward wind of the order of about 30 m/s and plasma movement driven by latitudinal gradient in electron density could lead an uplift of the F layer to height where the growth rate can trigger irregularities. The influence of wind and asymmetry of the EIA crests as well as perturbations from lower atmosphere, on the behavior of irregularities during the recovery phase of storms still require further investigations over Africa.

First result for the assessment of the capability of the PPEFM over the African longitude revealed that the model is capable of reproducing enhancement and reduction in the PRE caused by eastward and westward PPEF as well as the corresponding effect on the behavior of irregularities during storms. However, the model could not accurately reproduce long duration PPEF. One of the plausible reasons could be that during events characterized by long duration IMF Bz, DDEF might be active in addition to PPEF. A contributing factor could have also been the magnitude of auroral activity during such events (Huang, 2019). Nayak et al. (2016) had used the PPEFM to highlight the effect of eastward PPEF/ westward DDEF on the PRE thus, on the generation/inhibition of irregularities in the Indian/ Taiwanese sectors during the storm of 17 March 2015. Validating the PPEFM in the present study further reinforces the role of modeling in increasing our understanding of storm time electric field effect on irregularities over the low-latitude African sector**.**

5. Conclusions

The behavior of ionospheric irregularities over the crests of the African EIA in both hemispheres has been studied and the predictive capability of PPEFM along longitude 37^{o}E assessed during intense geomagnetic storms. It was found that:

1. Ionospheric irregularities over the magnetic equator and crests of the EIA were simultaneously suppressed by westward DDEF for over one hour on 23 April 2012, and subsequently triggered by an eastward PPEF from about 21:00 LT.

2. Similarly, irregularities were triggered by eastward PPEF that occurred at about 21:00 LT on 20 February 2014 as well as one hour earlier (20:00 LT) on 17 March 2013. They were inhibited thereafter (by westward DDEF) over the trough and crests.

3. The duration of irregularities inhibition during the recovery phases was related to the amplitude and duration of the magnetic perturbation Ddyn which lasted longer during the super storm of March 2015.

4. There was a hemispheric asymmetry in irregularities strength over the crests which might have been linked to the asymmetry in the magnitude and position of the EIA crests over Africa. In particular, the southern crests experienced irregularities on 16 July 2012 while the northern crest and trough did not. Also, irregularities were stronger (weaker) over the southern (northern) crest on 17 July 2012 and 15 November 2012 while on 19 March 2013, they were stronger in the southern crest and weaker in the trough and northern crest.

5. The PPEFM reproduced fairly well the PPEF that enhanced/reduced the PRE in the post sunset period during the main phase of storms of 17 March 2013/19 February 2014. It however, could not capture accurately the long duration PPEF which occurred on 15-16 June 2012 and 28-29 June 2013.

A better understanding of irregularities over the African EIA is however, limited by the absence of observational tools such as incoherent scatter radar (ISR) that could have given us more insight into the variations of electric field as well as the contribution of perturbation originating from the lower atmosphere during these events.

Acknowledgements

The authors wish to thank the ISGI (htpp://isgi.unistra.fr) for the SYM-H data; the ACE SWEPAM teams (http://www.srl.caltech.edu/ACE/ASC/level2/) for providing the IMF *Bz* and Vx data; the INTERMAGNET team (www.intermagnet.com) for the magnetometer data and UNAVCO (htpp://www.unavco.org/data/data.html) for the GNSS observables. The Prompt penetration equatorial electric field model data were obtained from http://www.geomag.org/models/PPEFM/ RealtimeEF.html. The CME catalog is generated and maintained at the CDAW Data Center by NASA and The Catholic University of America in cooperation with the Naval Research Laboratory. SOHO is a project of international cooperation between ESA and NASA. We finally appreciate the GFZ German Research Centre for Geosciences (ftp://ftp.gfz-potsdam.de) for making available the quiet days in each month. Solar flux and solar flare data were obtained from spaceweather.gc.ca and spaceweatherlive.com, respectively. The authors are also grateful to anonymous reviewers as well as the editor for their valuable comments which have substantially improved the quality of this manuscript.

References

Aarons, J., Mendillo, M., Yantosca, R., & Kudeki , E. (1996). GPS phase fluctuations in the equator region during the MISETA 1994 campaign. *Journal of Geophysical Research: Space Physics*, 101(A12), 26,851-26,862. https://doi.org/10.1029/96JA00981

Aarons, J. (1991). The role of the ring current in the generation or inhibition of equatorial F layer irregularities during magnetic storms. *Radio Science*, *26*(04), 1131-1149.

Aarons, J. (1982). Global Morphology of Ionospheric Scintillations, Proceeding of the IEEE. 70(4), 360-378.

Abdu, M. A. (2012). .Equatorial spread F/plasma bubble irregularities under storm time disturbance electric fields. *Journal of atmospheric and solar-terrestrial physics* 75, 44-56.

Abdu, M. A., Nogueira, P. A. B., Santos, A. M., de Souza, J. R., Batista, I. S., & Sobral, J. H. A.

(2018). Impact of disturbance electric fields in the evening on prereversal vertical drift and spread F developments in the equatorial ionosphere. *Annales Geophysicae*, 36, 609–620. https://doi.org/10.5194/angeo-36-609-2018

Abdu, M. A. (2012). Equatorial spread F/plasma bubble irregularities under storm time disturbance electric fields. *Journal of Atmospheric and Terrestrial Physics*, 75–76, 44–56.

Abdu, M. A., Kherani, E. A., Batista, I. S., & Sobral, J. H. A. (2009). Equatorial evening prereversal vertical drift and spread F suppression by disturbance penetration electric fields. *Geophysical Research Letters*, 36, L19103. https://doi.org/10.1029/2009GL039919

Abdu, M. A., Batista, I. S., Walker, G. O., Sobral, J. H. A., Trivedi, N. B., & De Paula, E. R. (1995). Equatorial ionospheric electric fields during magnetospheric disturbances: local time/longitude dependences from recent EITS campaigns. *Journal of Atmospheric and Terrestrial Physics*, *57*(10), 1065-1083. https://doi.org/10.1016/0021-9169(94)00123-6

Akala, A.O., Amaeshi, L.L.N., Doherty, P.H., Groves, K.M., Carrano, C. S., Bridgwood, C.T., & Seemala, G.K. (2014). Characterization of GNSS scintillations over Lagos, Nigeria during the minimum and ascending phases (2009–2011) of solar cycle 24. *Advances in Space Research*, 53, 37–47.

Amaechi, P. O., Oyeyemi, E. O., & Akala, A. O. (2018a). Geomagnetic storm effects on the occurrences of ionospheric irregularities over the African equatorial/low-latitude region, *Advances in Space Research*, 61, 2070–2090.

Amaechi, P. O., Oyeyemi, E. O., & Akala, A. O. (2018b). The response of African equatorial/low-latitude ionosphere to 2015 St. Patrick's Day geomagnetic storm. *Space Weather*, 16, 601–618. https://doi.org/10.1029/2017SW001751

Amory-Mazaudier, C., Bolaji, O. S., & Doumbia, V. (2017). On the historical origins of the CEJ, DP2, and Ddyn current systems and their roles in the predictions of ionospheric responses to geomagnetic storms at equatorial latitudes. *Journal of Geophysical Research: Space Physics*, 122, 7827–7833. https://doi.org/10.1002/2017JA024132

Appleton, E.V. (1946). Two anomalies in the ionosphere. *Nature*, 157(3995), 691.

doi:10.1038/157691a0

Astafyeva, E., Zakharenkova, I., Hozumi, K., Alken, P., Coïsson, P., Hairston, M. R., & Coley, W. R. (2018). Study of the Equatorial and Low-Latitude Electrodynamic and Ionospheric Disturbances During the 22–23 June 2015 Geomagnetic Storm Using Ground-Based and Spaceborne Techniques. *Journal of Geophysical Research: Space Physics*, *123*(3), 2424-2440. https://doi.org/10.1002/2017JA024981

Azzouzi, I., Migoya-Orue, Y., Amory-Mazaudier, C., Fleury, R., Radicella, S. M. & Touzani, A. (2015). Signature of solar event at middle and low latitudes in the European- African sector, during geomagnetic storms, October 2013. *Advances in Space Research*, 56(9), 2040– 2055. https://doi.org/10.1016/j.asr.2015.06.010

Basu, S., Groves, K. M., Quinn, J. M., & Doherty, P. (1999). A comparison of TEC fluctuations and scintillations at Ascension Island. *Journal of Atmospheric and Solar-Terrestrial Physics*, 61(16), 1219–1226. https://doi.org/10.1016/S1364-6826(99)00052-8

Blanc, M., & Richmond, A. D. (1980). The Ionospheric disturbance dynamo. *Journal of Geophysical Research: Space Physics*, 85(A4), 1669–1686. https://doi.org/ 10.1029/ JA085iA04p01669

Blewitt, G. (1990). An automatic editing algorithm for GPS data. *Geophysical Research Letters*, 17(2), 199–202. https://doi.org/10.1029/GL017i003p00199

Borries, C., Mahrous, A. M., Ellahouny, N. M., & Badeke, R. (2016). Multiple ionospheric perturbations during the Saint Patrick's Day storm 2015 in the European-African sector. *Journal of Geophysical Research: Space Physics*, 121, 11,333–11,345. https://doi.org/10.1002/2016JA023178

Carter, B. A., Retterer, J. M. Yizengaw, E., Groves, K., Caton, R., McNamara, L., et al. (2014). Geomagnetic control of equatorial plasma bubble activity modeled by the TIEGCM with Kp. *Geophysical Research. Letters*, 41, 5331–5339. https://doi.org/10.1002/ 2014GL060953

Chakrabarty, D., Sekar, R., Narayanan, R., Devasia, C. V & Pathan, B. M. (2005). Evidence for

the interplanetary electric field effect on the OI 630.0 nm airglow over low latitude. *Journal of Geophysical Research: Space Physics*, 110, A11301. https://doi.org/10.1029/2005JA011221

Chakraborty, M., Kumar, S., Guha, A., De, B. K. (2015). Effects of geomagnetic storm on low latitude ionospheric total electron content: A case study from Indian sector. Journal of Earth System Science 124(5), 1115-1126.

Chapman, S., & Ferraro, V. C. A. (1931). A new theory of magnetic storms. *Terrestrial Magnetism and Atmospheric Electricity*, 36, 77- 97.

Chapman, S. (1918). An outline of a theory of magnetic storms. *Proceedings of the Royal Society of London. Series A, Containing Papers of a Mathematical and Physical Character*, 95(666), 61-83.

Cole, K. D. (1966). Magnetic storms and associated phenomena. *Space Science Review*, 5, 699– 770.

Conker, R. S., El-Arini, M. B., Hegarty, C. J., & Hsiao, T. (2003). Modeling the effects of ionospheric scintillation on GPS/Satellite-Based Augmentation System availability.

Radio Science, 38(1), 1-1. https://doi.org/10.1029/2000RS002604

Danilov, A.D., & Lastovicka, J. (2001). Effects of geomagnetic storms on the ionosphere and atmosphere. *International Journal of Geomagnetism and Aeronomy*, 2, 209–224.

Datta-Barua, S., Su, Y., Deshpande, K., Miladinovich, D., Bust, G. S., Hampton, D., & Crowley, G. (2015). First light from a kilometer-baseline Scintillation Auroral GPS Array, *Geophysical Research Letters*, 42(10), 3639-3646.

Dugassa, T., Habarulema, J.B., & Nigussie, M. (2020). Statistical study of geomagnetic storm effects on the occurrence of ionospheric irregularities over equatorial/low-latitude region of Africa from 2001 to 2017, *Journal of Atmospheric and Solar-Terrestrial Physics* (2020), doi: https://doi.org/10.1016/j.jastp.2020.105198.

Eccles, J.V., St. Maurice, J.P., & Schunk, R.W. (2015). Mechanisms underlying the prereversal enhancement of the vertical plasma drift in the low latitude ionosphere. *Journal of Geophysical Research: Space Physics*, 120, 4950–4970.

Eccles, J. V. (2004). Assimilation of global-scale and mesoscale electric fields from low-latitude

satellites. *Radio Science*, 39, RS1S09.

Estey, L. H., & Meertens, C. M. (1999). TEQC: The multi-purpose toolkit for GPS/ GLONASS

data. *GPS Solutions*, 3(1), 42–49.

Farley, D. T., Balsey, B. B., Woodman, R. F., & McClure, J. P. (1970). Equatorial spread F: Implications of VHF radar observations. *Journal of Geophysical Research: Space Physics*, 75(34), 7199-7216. https://doi.org/10.1029/JA075i034p07199

Fathy, I., Amory-Mazaudier, C., Fathy, A., Mahrous, A. M., Yumoto, K., & Ghamry, E. (2014).

Ionospheric disturbance dynamo associated to a coronal hole: Case study of 5–10 April 2010. *Journal of Geophysical Research: Space Physics*, 119, 4120–4133. https://doi.org/ 10.1002/2013JA019510

Fejer, B.G., Jensen, J.W., & Su, S.Y. (2008). Quiet time equatorial F region vertical plasma drift model derived from ROCSAT-1 observations. *Journal of Geophysical Research: Space Physics*, 113, A05304.

Fejer, B.J., Scherliess, L., & de Paula, E.R. (1999). Effects of the vertical plasma drift velocity

on the generation and evolution of equatorial spread F. *Journal of Geophysical Research: Space Physics*, 104 (A9), 19859-19,869. https://doi.org/10.1029/1999JA900271

Fejer,B.G., & Scherliess, L. (1997). Empirical models of storm time equatorial zonal electric fields. *Journal of Geophysical Research: Space Physics*, 102, AII, 24,047-24,056. https://doi.org/10.1029/97JA02164

Fejer, B. G., & Scherliess, L. (1995). Time dependent response of equatorial ionospheric electric fields to magnetospheric disturbances. *Geophysical Research Letters*, *22*(7), 851–854. https://doi.org/10.1029/95GL00390

Groves, K.M., Basu, S., Weber, E. J., Smithan, M., Kuenzler, H., Valladares, C. E., et al. (1997). Equatorial scintillation and system support. *Radio Science*, 32, 2047–2064.

Haerendel, G. (1973). Theory of equatorial spread F. *R*eport. *Max-Planck Instute for Physics and Astrophysics, Garching, Germany*.

Hansen, A., Blanch, J., & Walter, T. (2000). Ionospheric correction analysis for WAAS quiet and stormy (pp. 634–642). ION GPS, Salt Lake City, Utah, September 19-22.

Huang, C. S. (2019). Long-Lasting Penetration Electric Fields during Geomagnetic Storms: Observations and Mechanisms. *Journal of Geophysical Research: Space Physics*, 124, 11, 9640-9664. https://doi.org/10.1029/2019JA026793

Huang, C-S. (2018). Effects of Geomagnetic Storms on the Postsunset Vertical Plasma Drift in the Equatorial Ionosphere. *Journal of Geophysical Research: Space Physics*, 123, 5. https://doi.org/10.1029/2018JA025360

Huang, C. M. (2013). Disturbance dynamo electric fields in response to geomagnetic storms at different universal times. *Journal of Geophysical Research: Space Physics*, 118, 496–501, https://doi:10.1029/2012JA018118.

Huang, C.-S., Rich, F. J. & Burke, W. J. (2010). Storm time electric fields in the equatorial ionosphere observed near the dusk meridian. *Journal of Geophysical Research: Space Physics*, 115, A08313. https://doi:10.1029/2009JA015150

Huang, C.-S., Foster, J. C. & Kelley, M. C. (2005). Long-duration penetration of the interplanetary electric field to the low-latitude ionosphere during the main phase of magnetic storms. *Journal of Geophysical Research: Space Physics*, 110, A11309. https://doi:10.1029/2005JA011202.

Jacobsen, K.S., & Dähnn, M. (2014). Statistics of ionospheric disturbances and their correlation with GNSS positioning errors at high latitudes. *Journal of Space Weather and Space Climate*, 4, A27.

Joshi, L. M., Balwada, S., Pant, T. K., & Sumod, S. G. (2015). Investigation on F layer height rise and equatorial spread F onset time: Signature of standing large-scale wave. *Space Weather*, 13(4), 211-219.

Kalita, B. R., Hazarika, R., Kakoti, G., Bhuyan, P. K., Chakrabarty, D., Seemala, G. H. et al. (2016). Conjugate hemisphere ionospheric response to the St. Patrick's Day storms of 2013 and 2015 in the 100°E longitude sector. *Journal of Geophysical Research: Space Physics*, 121, 11. https://doi.org/10.1002/2016JA023119

Kamide, Y., & Fukushima, N. (1972). Positive geomagnetic bays in evening high latitudes and their possible connection with partial ring current. *Report of Ionosphere and Space Research in Jap*an, 26, 79-101.

Kassa, T., & Damtie, B. (2017). Ionospheric irregularities over Bahir Dar, Ethiopia during selected geomagnetic storms. *Advances in Space Research*, 60(1), 121–129.

Kelley, M. C. (1989a). *The Earth's ionosphere. Plasma physics and electrodynamics, International Geophysics series* (Vol. 43). Academic Press.

Kelley, M. C. (1989b). *Ionospheric Radio*. Peter Peregrinus Ltd. London.

Kelley, M. C., Fejer, B. G., & Gonzales, C. A. (1979). An explanation for anomalous equatorial ionospheric electric fields associated with a northward turning of the interplanetary magnetic field. *Geophysical Research Letters*, 6, 301–304.

Kikuchi, T., Hashimoto, K. K., & Nozaki, K. (2008). Penetration of magnetospheric electric

fields to the equator during a geomagnetic storm. *Journal of Geophysical Research: Space Physics*, 113(A6). https://doi.org/10.1029/2007JA012628

Kikuchi, T., Hashimoto, K., Kitamura, T.-I., Tachihara, H., & Fejer, B. (2003). Equatorial counter electrojets during substorms. *Journal of Geophysical Research: Space Physics*, 108(A11), 1406. https:// doi:10.1029/2003JA009915

Kikuchi, T., Lühr, H., Schlegel, K., Tachihara, H., Shinohara, M., & Kitamura, T. I. (2000). Penetration of auroral electric fields to the equator during a substorm. *Journal of Geophysical Research: Space Physics*, 105, 23,251–23,261. https://doi.org/10.1029/2000JA90001

Kikuchi, T., & Araki, T. (1979). Transient response of uniform ionosphere and preliminary reverse impulse of geomagnetic storm sudden commencement. *Journal of Atmospheric and Terrestrial Physics*, 41, 917–925.

Kintner, P.M., Ledvina, B. M., & de Paula, E. R. (2007). GPS and ionospheric scintillations. *Space Weather*, 5, S09003.

Kuznetsov, B. M., & Troshichev, O. A. (1977). On the nature of polar cap magnetic activity during undisturbed periods. *Planet Space Science*, 25(1), 15-21.

Le-Huy, M., & Amory-Mazaudier, C. (2005). Magnetic signature of the ionospheric disturbance dynamo at equatorial latitudes, "Ddyn". *Journal of Geophysical Research: Space Physics*, 10, A10301. https://doi.org/10.1029/2004JA010578

Le Huy, M., & Amory-Mazaudier, C. (2008). Planetary magnetic signature of the storm wind disturbance dynamo currents: Ddyn. *Journal of Geophysical Research: Space Physics*, 113, A02312. https://doi.org/10.1029/2007JA012686

Ma, G., & Maruyama, T. (2006). A super bubble detected by dense GPS network at East Asian longitudes. *Geophysical Research Letters*, 33, L21103.

Mannucci, A. J., Wilson, B. D., & Edwards, C. D. (1993). A new method for monitoring the Earth's ionosphere total electron content using the GPS global network. Proceedings of ION GPS-93, Institute of Navigation (pp. 1323–1332).

Manoj, C. S. M., Maus, S., Lühr, H., & Alken, P. (2008). Penetration characteristics of the interplanetary electric field to the day-time equatorial ionosphere. *Journal of Geophysical Research Atmosphere*, 113(A12). https://doi.org/10.1029/2008JA013381

Manoj, C., & Maus, S. (2012). A real-time forecast service for the ionospheric equatorial zonal electric field. *Space Weather*, 10(9), 1-9.

Maruyama, T., & Matuura, N. (1984). Longitudinal variability of annual changes in activity of equatorial spread F and plasma bubbles. *Journal of Geophysical Research: Space Physics*, 39, 10903–10912. https://doi.org/10.1002/2015JA022299

Mayaud, P. N. (1965). Analyse morphologique de la variabilité jour-à-jour de la variation journalière régulière SR du champ magnétique terrestre, I- le système de courants Cp (régions polaires et subpolaires). *Annales Geophysicae*, 21, 369-401.

Mungufeni, P., Habarulema, J.B., & Jurua, E. (2016). Trends of ionospheric irregularities over African low latitude region during quiet time geomagnetic conditions. *Journal of*

Atmospheric and Terrestrial Physics, 138–139, 261–267.

Namba, S., & Maeda, K.-I. (1939). Radio Wave Propagation, 86 pp., Corona, Tokyo.

Nava, B., Rodríguez-Zuluaga, J., Alazo-Cuartas, K., Kashcheyev, A., Migoya-Orué, Y., Radicella, S. M., et al. (2016). Middle and low latitude ionosphere response to 2015 St. Patrick's Day geomagnetic storm. *Journal of Geophysical Research: Space Physics*, 121, 3421–3438. https://doi.org/10.1002/2015JA022299

Nayak, C., Tsai, L.-C., Su, S.-Y., Galkin, I., Caton, R., & Groves, K. (2016). Suppression of ionospheric scintillation during St. Patrick's 24 Day geomagnetic super storm as observed over the anomaly crest region station Pingtung, Taiwan: A case study. *Advances in Space Research*, 60, 396-405.

Nicolls, M. J., Kelley, M. C., Vlasov, M. N., Sahai, Y., Chau, J. L., Hysell, D. L., et al. (2006). Observations and modeling of post-midnight uplifts near the magnetic equator. *Annales Geophysicae*, 24, 1317–1331.

Nishida, A., Iwasaki, N., & Nagata, T. (1966). The origin of fluctuation in the equatorial elecyrojet: a new type of geomagnetic variation. *Annales Geophysicae*, 22, 478.

Nishida, A. (1968). Geomagnetic DP2 fluctuations and associated magnetospheric Phenomena.

Journal of Geophysical Research: Space Physics, 73, 1795–1803. https://doi.org/10.1029/ JA073i005p01795

Ngwira, C. M., Klenzing, J., Olwendo, J., D'ujanga, F. M., Stoneback, R., & Baki, P. (2013). A study of intense ionospheric scintillation observed during a quiet day in the East African low-latitude region. *Radio Science*, 48, 396–405.

Oladipo, O.A., Adeniji, J.O., Olawepo, A.O., & Doherty, P.H. (2013). Large-scale ionospheric irregularities occurrence at Ilorin, Nigeria. *Space Weather*, 12, 300-305.

Olwendo, O. J., Yamazak, Y., Cilliers, P., Baki, P., Ngwira, C. M., & Mito, C. (2015). A study on the response of the Equatorial Ionization Anomaly over the East Africa sector during the geomagnetic storm of November 13, 2012. *Advances in Space Research*, *55*(12), 2863-2872.

Olwendo, O. J., Baluku, T., Baki, P., Cilliers, P. J., Mito, C., & Doherty, P. (2013). Low latitude ionospheric scintillation and zonal irregularity drifts observed with GPS-SCINDA system and closely spaced VHF receivers in Kenya. *Advances in Space Research*, *51*(9), 1715-1726.

Ossakow, S. L. (1981). Spread-F theories–A review. *Journal of Atmospheric and Solar Terrestrial Physics*, 43, 437-443.

Otsuka, Y., Suzuki, K., Nakagawa, S., Nishioka, M., Shiokawa, K., & Tsugawa, T. (2013). GPS observations of medium-scale traveling ionospheric disturbances over europe. *Annales Geophysicae*, 31(2), 163–172.

Ott, E. (1978). Theory of Rayleigh-Taylor bubbles in the equatorial ionosphere. *Journal of Geophysical Research: Space Physics*, 83(A5), 2066-2070. https://doi.org/10.1029/JA083iA05p02066.

Paznukhov, V. V., Carrano, C. S., Doherty, P. H., Groves, K. M., Caton, R. G., Valladares, C. E., et al. (2012). Equatorial plasma bubbles and L-band scintillations in Africa during solar minimum. *Annales Geophysicae*, 30, 675–682.

Perkins, F. W. (1975). Ionospheric irregularities. Review of Geophysical, 13(3), 884.

https://doi.org/10.1029/RG018i002p00401

Pi, X., Manucci, A. J., Lindqwister, U. J., & Ho, C. M. (1997). Monitoring of global ionospheric irregularities using the worldwide GPS network, Geophys. Res. Lett., 24, 2283–2286.

Rama Rao, P.V. S., Niranjan, K., Prasad, D.S.V.V.D., Gopi, S. K., & Uma, G. (2006). On the validity of the ionospheric pierce point (IPP) altitude of 350 km in the Indian equatorial and low-latitude sector. *Annales Geophysicae*, 24, 2159–2168.

Rostoker, G. A. (1967). Determining factor in the form of the equivalent current system for geomagnetic bays. *Earths Planetary Science Letters*, 2, 119.

Rostoker, G. (1969). Classification of Polar magnetic disturbances. *Journal of Geophysical Research*, 74(21), 5161. https://doi.org/10.1029/JA074i021p05161.

Sabaka, T. J., Olsen, N., & Purucker, M. E. (2004). Extending comprehensive models of the Earth magnetic field with Oersted and Champ data. *Geophysical Journal International*, 159(2), 521–547.

Sardon, E., Rius, A., & Zarraoa, N. (1994). Estimation of the transmitter and receiver differential biases and the ionospheric total electron content from GPS observations. *Radio Science*, 29(3), 577–586.

Seba, E.B., & Nigussie, M. (2016). Investigating the effect of geomagnetic storm and equatorial electrojet on equatorial ionospheric irregularity over east african sector. *Advances in Space Research*, 58, 1708–1719.

Seemela, G. K. (2010). Rinex GPS-TEC program, version 1.45. satellite navig. sci and tech for Africa. In: Presentation at a Workshop held from 23rd March–9th April, 2009 at ICTP, Trieste, Italy.

Seemala, G.K., & Valladares, C. E. (2011). Statistics of TEC depletions observed over the South

American continent for the year 2008. *Radio. Science*, 46, RS5019.

Scherliess, L & Fejer, B.G. (1997). Storm time dependence of equatorial disturbance dynamo zonal electric fields. *Journal of geophysical research*, 102 (All), 24,037-24,046.

Shreedevi, P. R., & Choudhary, R. K. (2017). Impact of oscillating IMF *Bz* during 17 March 2013 storm on the distribution of plasma over Indian low-latitude and mid-latitude ionospheric regions. *Journal of Geophysical Research: Space Physics*, *122*, 11,607–11,623.

https://doi.org/10.1002/2017JA023980

Stauning, P. (2012). The Polar Cap PC Indices: Relations to Solar Wind and Global Disturbances, Exploring the Solar Wind, Dr. Marian Lazar (Ed.), ISBN: 978-953-51-0339-4.

Sultan, P. J. (1996). Linear theory and modeling of the Rayleigh-Taylor instability leading to the occurrence of equatorial spread F. *Journal of Geophysical Research: Space Physics*, 101(A12), 26,875-26,891. https://doi.org/10.1029/96JA00682.

Sunda, S., Sridharan, R., Vyas, B. M., Khekale, P. V., Parikh, K. S., Ganeshan, A. S., et al. (2015). Satellite-based augmentation systems: A novel and cost-effective tool for ionospheric and space weather studies. *Space Weather*, 13(1), 6-15.

Svalgaard, L. (1968). Sector structure of the interplanetary magnetic field and daily variation of

the geomagnetic field at high-latitudes. Danish. Meteor. *Geophysical Paper*, R-6.

Tesema, F., Mesquita, R., Meriwether, J., Damtie, B., Nigussie, M., Makela, J., et al. (2017). New results on equatorial thermospheric winds and temperatures from Ethiopia, Africa. *Annales Geophysicae,* 35(2), 333-344.

Troschichev, O., & Janzhura, A. (2012). Space Weather Monitoring by Ground-Based Means:

PC Index. Springer, Chichester, UK.

Tsunoda, R. T., Thampi, S. V., Nguyen, T. T., & Yamamoto, M. (2013). On validating the relationship of ionogram signatures to large-scale wave structure. *Journal of Atmospheric and Solar Terrestrial Physics*, 103, 30-35.

Tsunoda, R.T. (1985). Control of the seasonal and longitudinal occurrence of equatorial scintillations by the longitudinal gradient in integrated E region Pedersen conductivity. *Journal of Geophysical Research: Space Physics,* 90 (A1), 447–456.

Vasyliunas, V. M. (1970). Mathematical models of magnetospheric convection and its coupling

to the ionosphere. In Particles and Fields in the Magnetosphere (pp. 60-71). Springer, Dordrecht.

Wanliss, J.A., & Showalter, K. M. (2006). High-resolution global storm index: Dst versus SYM-H. *Journal of Geophysical Research: Space Physics,* 111(A2), A02202. https://doi.org/10.1029/2005JA011034.

Wiens, R.H., Ledvina, B.M., Kintner, P.M., Afewerki, M., & Mulugheta, Z., (2006). Equatorial plasma bubbles in the ionosphere over Eritrea: occurrence and drift speed. *Annales Geophysicae*, 24, 1443–1453.

Yamazaki, Y., & Kosch, M. J. (2015). The equatorial electrojet during geomagnetic storms and

substorms. *Journal of Geophysical Research: Space Physics,* 120, 2276–2287. https://doi.org/10.1002/2014JA020773

Yizengaw, E., & Groves, K. M (2018). Longitudinal and Seasonal Variability of Equatorial Ionospheric Irregularities and Electrodynamics. *Space Weather*, 16(8), 946-968.

Yizengaw, E., Moldwin, M.B., Zesta, E., Bioele, C.M., Damtie, B., Mebrahtu, A., Rabiu, B., Valladares, C.F., & Stoneback, R., (2014). The longitudinal variability of equatorial electrojet and vertical drift in the African and American sectors. *Annales Geophysicae*, 32, 231–238.

Yizengaw, E., Retterer, J., Pacheco, E. E., Roddy, P., Groves, K., Caton, R., & Baki, P. (2013a).

Post-midnight Bubbles and Scintillations in the Quiet-Time June Solstice. *Geophysical Research Letters*, 40, 5592-5597.

Yizengaw, E., Doherty, P., & Fuller-Rowell, T. (2013b). Is Space Weather Different Over Africa, and If so, Why? AGU Chapman Conference Report. *Space Weather*, 398-391.

Yue, X., Schreiner, W. S., Kuo, Y. H., & Lei, J. (2015). Ionosphere equatorial ionization anomaly observed by GPS radio occultation during 2006–2014. *Journal of Atmospheric and Terrestrial Physics*, 129, 30-40.

Zakharenkova, I., Cherniak, I., & Krankowski, A. (2019). Features of storm-induced ionospheric irregularities from ground-based and spaceborne GPS observations during

the 2015 St. Patrick's Day storm. *Journal of Geophysical Research: Space Physics*.

Zakharenkova, I., & Astafyeva, E. (2015). Topside ionospheric irregularities as seen from multisatellite observations. *Journal of Geophysical Research: Space Physics*, *120*(1), 807-824.

Zaourar, N., Amory-Mazaudier, C., & Fleury, R. (2017). Hemispheric asymmetries in the ionosphere response observed during the high-speed solar wind streams of the 24-28 August 2010. *Advances in Space Research*, 59(9), 2229-2247. https://doi.org/10.1016/j.asr. 2017. 01.048.

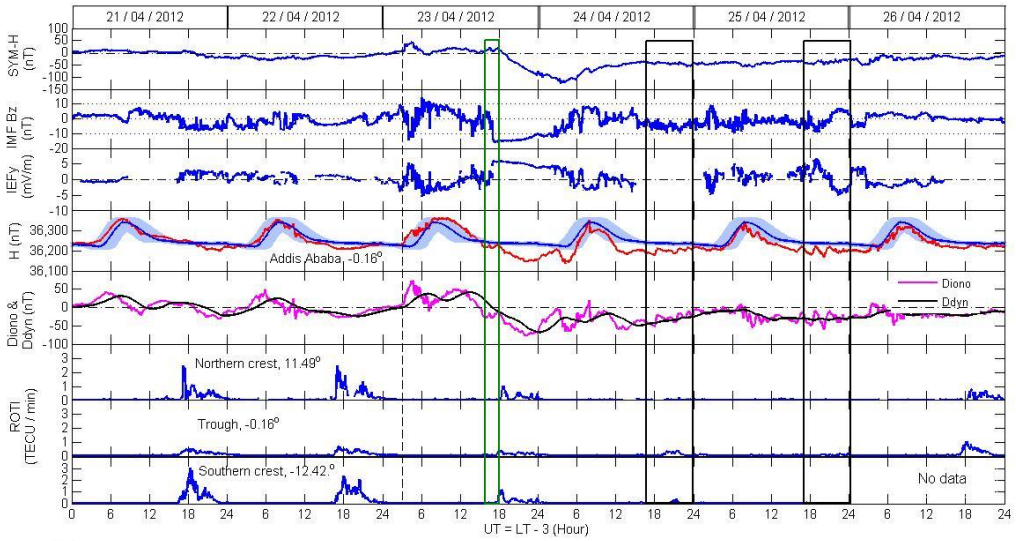

Figure 1: Variations of SYM-H, IMF Bz, IEFy, H, Diono, Ddyn and ROTI over the crests and trough of the African EIA from 21 – 26 April 2012. The broken vertical line indicates the time of sudden storm commencement. In panel 4, the light blue area represents the limit of day-by-day variation of H, the tick blue line is the regular variation of H while the red line is the observed H.

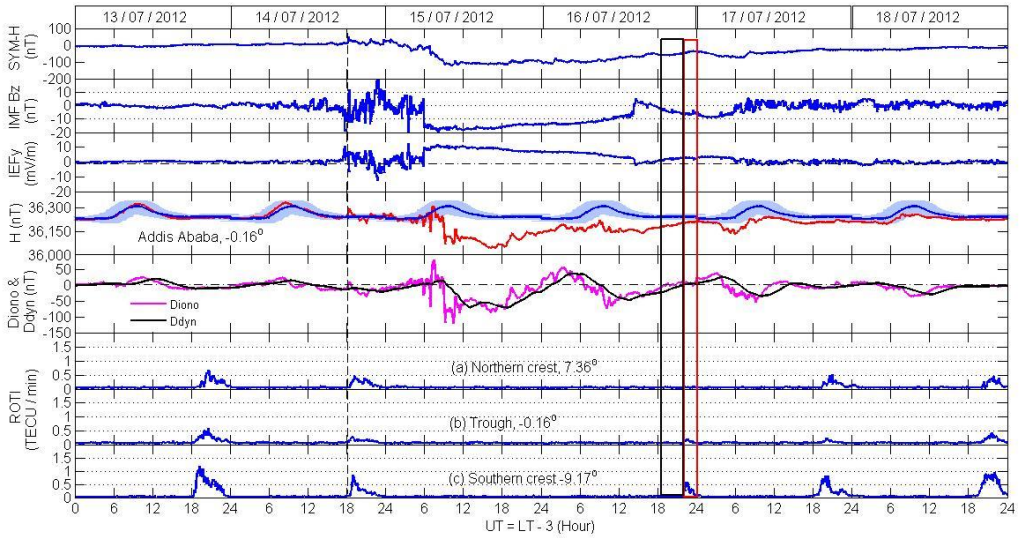

Figure 2: Variations of SYM-H, IMF Bz, IEFy, H, Diono, Ddyn and ROTI over the crests and trough of the African EIA from 13 – 18 July 2012.

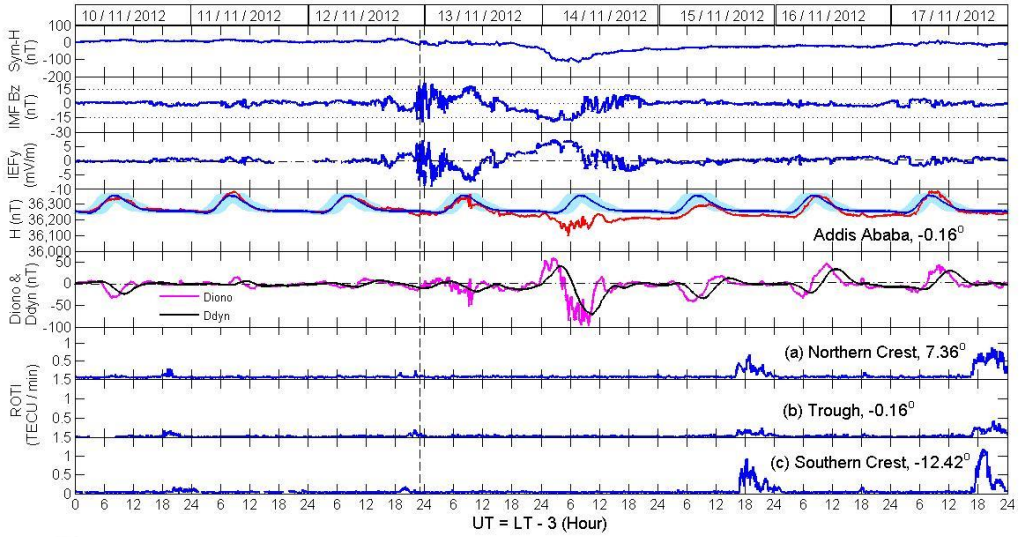

Figure 3: Variations of SYM-H, IMF Bz, IEFy, H, Diono, Ddyn and ROTI over the crests and trough of the African EIA from 10 – 17 November 2012.

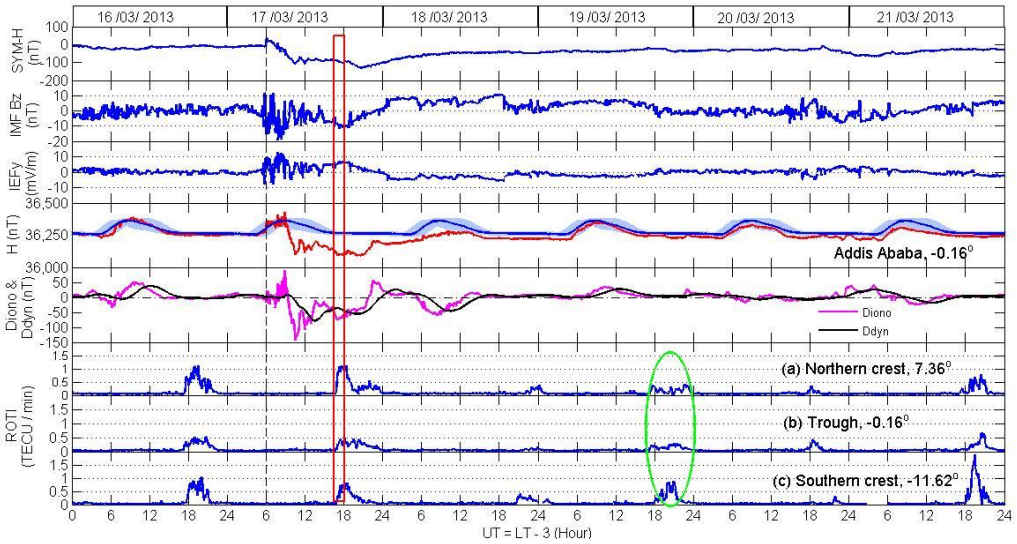

Figure 4: Variations of SYM-H, IMF Bz, IEFy, H, Diono, Ddyn and ROTI over the crests and trough of the African EIA from 16 – 21 March 2013.

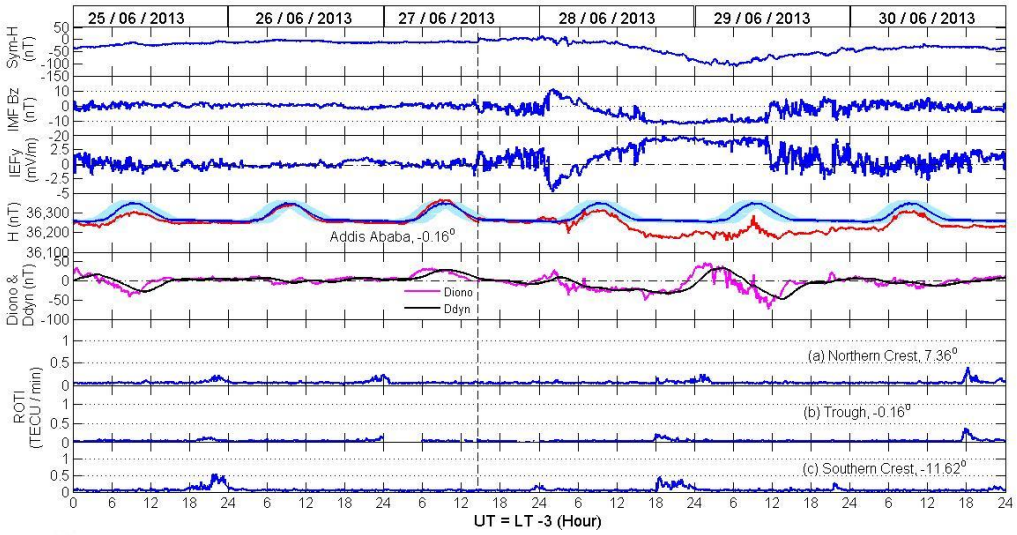

Figure 5: Variations of SYM-H, IMF Bz, IEFy, H, Diono, Ddyn and ROTI over the crests and trough of the African EIA from 25 – 30 June 2013.

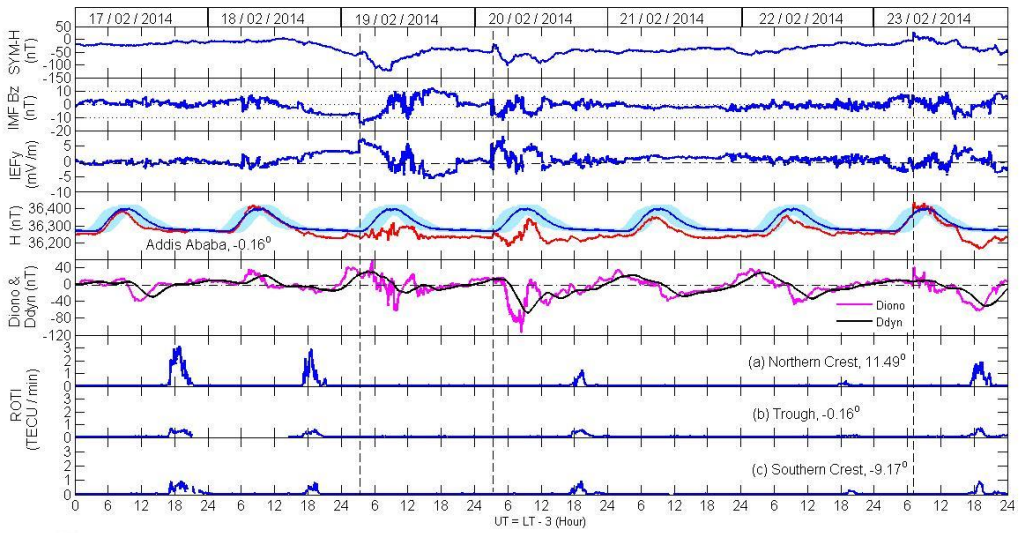

Figure 6: Variations of SYM-H, IMF Bz, IEFy, H, Diono, Ddyn and ROTI over the crests and trough of the African EIA from 17 – 23 February 2014.

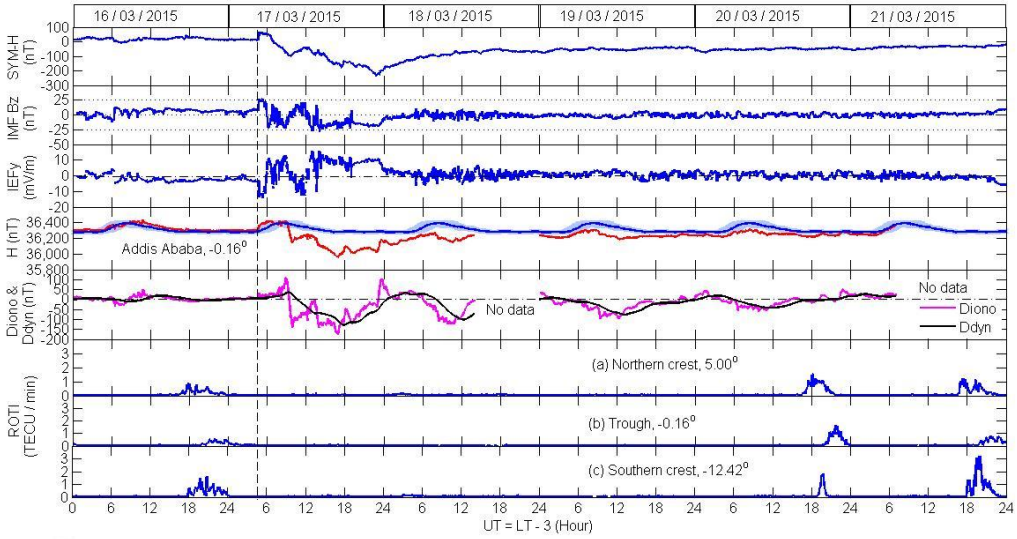

Figure 7: Variations of SYM-H, IMF Bz, IEFy, H, Diono, Ddyn and ROTI over the crests and trough of the African EIA from 16 – 21 March 2015.

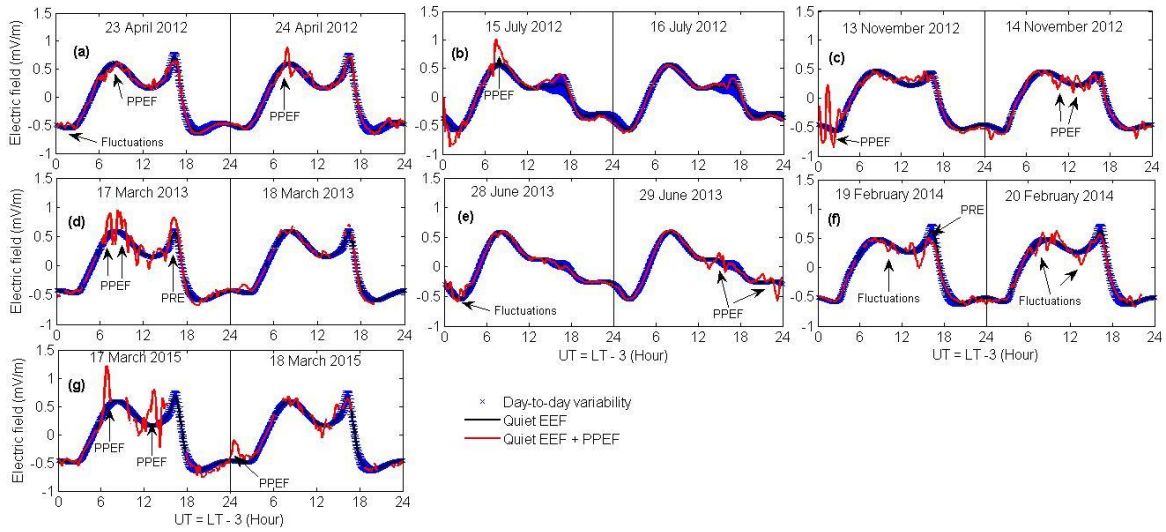

Figure 8: Effects of PPEFs over the African longitude (37^{o}E) during the main phase of the storms.

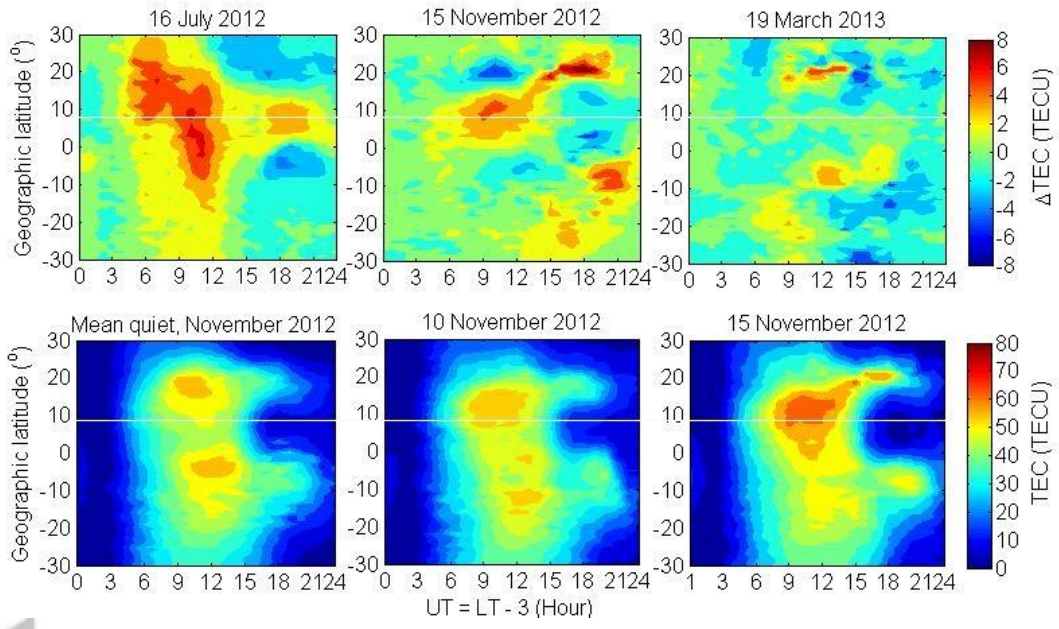

Figure 9: Variation of perturbation TEC (ΔTEC) on 16 July 2012, 15 November 2012 and 19 March 2013 (first panel) and TEC on 11 and 15 November 2012 (Second panel). The profiles are for mean longitude 37ºE with latitudinal coverage of ±30º and the white lines represent the magnetic equator.

Table 1: Coordinates of the GNSS and magnetometer station.

Station / Country	Station code	Geo. Lat	Geo. Lon	Geo. Mag. Lat
	GPS Station			
Mitzpe Ramon, Israel	ramo	30.60° N	34.76° E	23.38°
Halat Ammar, Saudi Arabia	haly	29.16° N	36.07° E	21.87°
Al Wajh, Saudi Arabia	alwj	26.46° N	36.38° E	18.73°
Sola village, Saudi Arabia	sola	24.91° N	46.40° E	17.71°
Nama, Saudi Arabia	nama	19.21° N	42.05° E	11.49°
Sheba, Eritrea	sheb	15.85° N	39.05° E	7.36°
Asab, Eritrea	asab	13.06° N	42.65° E	4.91°
Addis Ababa, Ethiopia	adis	9.03° N	38.77° E	-0.16°
Nazret, Ethiopia	nazr	8.57° N	39.29° E	-0.25°
Negele, Ethiopia	nege	5.33° N	39.59° E	-3.60°
Eldoret, Kenya	moiu	0.29° N	35.29° E	-9.17°
Entebbe, Uganda	ebbe	0.05° N	32.44° E	-9.52°
Mbarara, Uganda	mbar	0.60° S	30.74° E	-10.22°
Kigali, Rwanda	nurk	1.94° S	30.09° E	-11.62°
Malindi, Kenya	mal2	2.99° S	40.19° E	-12.42°
Dodoma, Tanzania	dodm	6.17° S	35.75° E	-16.08°
Tanzania, Tanzania	tanz	-8.57° S	39.29° E	-18.55°
Tuckuya, Tanzania	tuck	-9.33° S	33.75° E	-19.51°
Mzuzu, Malawi	mzuz	11.43° S	34.00° E	-21.88°
Zambia, Zambia	zamb	15.43° S	28.31° E	-23.78°
Ngamiland, Botswana	maua	19.19° S	23.85° E	-30.11°
Hartebeesthoek, South Africa	hrao	25.89° S	27.68° E	-36.32°
Sutherland, South Africa	suth	32.38° S	20.81° E	-41.10°
	Magnetometer station			
Addis Ababa, Ethiopia	AAE	9.04° N	38.77° E	0.16°

Table 2: Amplitude of Diono and Ddyn minima

Storm	Day	Diono (nT) & Time (UT)	Ddyn (nT) & Time (UT)
Event 1 (2012)	23 April	-28.7 (16:46); -77.0 (22:06)	----
	24 April	-64.6 (04:46); -60.3 (12:23)	-67.6 (00:20); -49.7 (15:27)
	25 April	-54.5 (09:00); -56.4 (20:00)	-34.0 (12:42)
Event 2 (2012)	14 July	-35.3 (21:40)	
	15 July	-116.5 (09:11); -117.4 (10:30); -86.4 (16.14)	-68.7 (12:48); -70.7 (18:46)
	16 July	-71.4 (10:09 UT)	-46.3 (13:25)
	17 July	-53.0 (09:13 UT)	-33.3 (10:18)
	18 July	-34.0 (09:05 UT)	-28.0 (12:21)
Event 3 (2012)	10 November	-31.6 (08:00)	-23.7 (10:15)
	13 November	-52.4 (10:15)	-14.0 (19:54)
	14 November	-85.2 (05:38); -92.8 (09:53)	-69.1 (10:51)
	15 November	-41.8 (07:10)	-33.26 (09:39)
	16 November	-31.2 (05:55)	-20.5 (07:56)
Event 4 (2013)	17 March	-137.7 (10:27); -107.4 (11:57); -74.7 (17:07)	-78.7 (13:30); -54.0 (20:40)
	18 March	-59.5 (08:17)	-45.6 (10:22)
Event 5 (2013)	25 June	-41.7 (08:40)	-26.4 (11.37)
	28 June	-36.92 (04:31); -49.7 (16:25)	-33.0 (20:02)
	29 June	-72.4 (11:24)	-48.0 (13:27)
Event 6 (2014)	19 February	-61.5 (09:50)	-19.8 (11:55)
	20 February	-111.9 (08:28)	-66.5 (09:47)
	21 February	-39.2 (10:52)	-28.1 (13:28)
	22 February	-48.1 (09:35)	-33.8 (12:51)
	23 February	-61.7 (18:51)	-50.6 (20:26)
Event 7 (2015)	17 March	-140.4 (09:54); -173.4 (16:56); -114.3 (19:19)	-127.30 (17:41)
	18 March	-122.2 (10:14)	-101.0 (12:24)
	19 March	-98.1 (12:13)	-75.4 (13:24)
	20 March	-60.0 (09:50)	-42.2 (11:46)